6

Formation of kinks

In this chapter we study the formation of kinks and domain walls during a phase transition. We start by describing the effective potential for a field theory at finite temperature. This sets up a useful framework for discussing phase transitions and defect formation.

6.1 Effective potential

The effective potential is a tool that is often used to study phase transitions in field theory [89, 179, 90, 47, 100]. The idea is to consider the interaction of a scalar degree of freedom ("order parameter") with a thermal background of particles. Such processes induce additional temperature dependent terms in the potential for the order parameter, leading to an "effective potential." The shape of the effective potential varies as a function of temperature and new minima might appear. The global minimum defines the vacuum of the model. If a new global minimum appears at some temperature, it indicates that the system makes a transition to a new expectation value of the order parameter and there is a phase change. We now describe the (one loop) effective potential in a little more detail.

We consider a field theory of scalar, spinor and vector fields

$$L = L_{\mathrm{B}} + L_{\mathrm{F}} \tag{6.1}$$

with the bosonic Lagrangian

$$L_{\mathrm{B}} = \frac{1}{2}(\mathrm{D}_\mu \Phi_i)\mathrm{D}^\mu \Phi_i - V(\Phi) - \frac{1}{4}F^a_{\mu\nu}F^{\mu\nu a} \tag{6.2}$$

where Φ_i are the components of the scalar fields,

$$\mathrm{D}_\mu \equiv \partial_\mu - \mathrm{i}eA^a_\mu T^a \tag{6.3}$$

https://doi.org/10.1017/9781009290456.007 Published online by Cambridge University Press

the T^a are group generators, and

$$F^a_{\mu\nu} \equiv \partial_\mu A^a_\nu - \partial_\nu A^a_\mu + \mathrm{e} f^{abc} A^b_\mu A^c_\nu \tag{6.4}$$

where A^a_μ are the gauge fields.

The Lagrangian for a fermionic multiplet Ψ is

$$L_\mathrm{F} = \mathrm{i}\bar{\Psi}\gamma^\mu \mathrm{D}_\mu \Psi - \bar{\Psi}\Gamma_i \Psi \Phi_i \tag{6.5}$$

where Γ_i are the Yukawa coupling matrices. The quantity Ψ denotes a collection of fermionic fields and the Yukawa coupling term may be written more explicitly as $\bar{\Psi}^\sigma_\alpha \Gamma^{\alpha\beta}_{i\sigma\rho} \Psi^\rho_\beta \Phi_i$ where α, β label the various fermionic fields, the superscripts σ, ρ on the fermion fields are spinor indices, and i labels the interaction term with the scalar field Φ_i. Γ_i has spinor indices because it could contain the unit matrix (vector coupling) and/or the γ^5 matrix (axial coupling) defined in Eq. (5.17).

If the expectation values of the scalar fields are denoted by Φ_{0i}, then the mass matrices of the various fields are written as

$$\mu^2_{ij} = \left.\frac{\partial^2 V}{\partial\Phi_i \partial\Phi_j}\right|_{\Phi=\Phi_0}, \quad \text{scalar fields} \tag{6.6}$$

$$m = \Gamma_i \Phi_{0i}, \quad \text{spinor fields} \tag{6.7}$$

$$M^2_{ab} = e^2 (T_a T_b)_{ij} \Phi_{0i} \Phi_{0j}, \quad \text{vector fields} \tag{6.8}$$

where a, b are gauge field group indices.

Then the finite temperature, one loop effective potential is[1]

$$V_\mathrm{eff}(\Phi_0, T) = V(\Phi_0) + \frac{\mathcal{M}^2}{24} T^2 - \frac{\pi^2}{90} \mathcal{N} T^4 \tag{6.9}$$

where

$$\mathcal{N} = \mathcal{N}_\mathrm{B} + \frac{7}{8} \mathcal{N}_\mathrm{F} \tag{6.10}$$

is the number of bosonic and fermionic spin states, and

$$\mathcal{M}^2 = \mathrm{Tr}(\mu^2) + 3\mathrm{Tr}(M^2) + \frac{1}{2}\mathrm{Tr}(\gamma^0 m \gamma^0 m) \tag{6.11}$$

where γ^0 is defined in Eq. (5.15). Note that $\mathcal{M}^2$ depends on the expectation value Φ_0 through the defining equations for the mass matrices given above. For example, $\mathcal{M}^2$ contains a term proportional to $\mathrm{Tr}(\Phi_0^2)$.

An important feature of the effective potential is that it can show the presence of phase transitions. If there are scalar fields with negative mass squared terms in

[1] Radiative corrections and spontaneous symmetry breaking are discussed in [33, 178].

https://doi.org/10.1017/9781009290456.007 Published online by Cambridge University Press

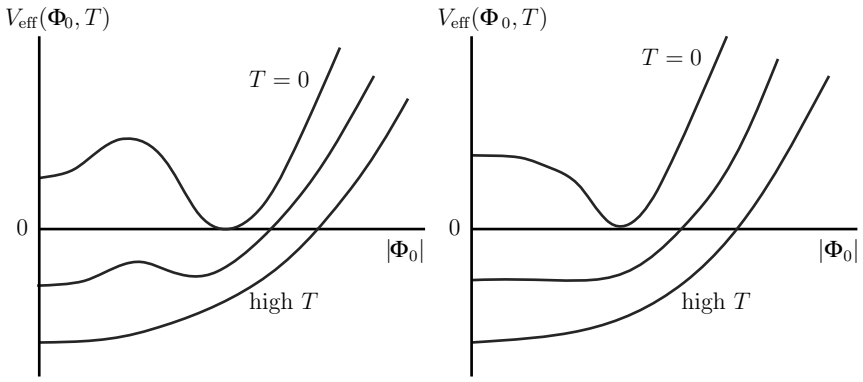

Figure 6.1 Sketch of effective potential for first-order phase transition (left) and second-order phase transition (right). In the first-order case, the global minimum of the potential at high temperature ($\Phi_0 = 0$ in illustration) becomes a local minimum at low temperature. In the second-order case, the global minimum of the potential at high temperature becomes a local maximum at low temperature. The effective potential at $\Phi_0 = 0$ decreases with increasing temperature because of the last term proportional to $-\mathcal{N}T^4$ in Eq. (6.9).

$V(\Phi)$, the contributions from the $\mathcal{M}^2T^2$ term in the effective potential, Eq. (6.9), can make the effective mass squared positive for these fields if the temperature is high enough (see Fig. 6.1). Therefore when the system is at high temperature, the effective mass squared can be positive and the minimum of the potential at $\Phi_0 = 0$. As the system is cooled, the effective mass squared becomes negative and the minimum of the effective potential occurs at non-zero values of Φ_0 and the lowest energy state has shifted from $\Phi_0 = 0$ to $\Phi_0 \neq 0$. The order parameter, Φ, acquires a non-zero "vacuum expectation value" at some critical temperature. This is the phenomenon of spontaneous symmetry breaking and manifests itself as a phase transition. The phase at high temperature had a certain symmetry dictated by the invariance of the field theory with $\Phi_0 = 0$ and at low temperature the symmetry is changed because now $\Phi_0 \neq 0$.

As a simple example of an effective potential, consider the $\lambda\phi^4$ model of Eq. (1.2) with

$$V(\phi) = -\frac{m_0^2}{2}\phi^2 + \frac{\lambda}{4}\phi^4 + \frac{\lambda}{4}\eta^4 \tag{6.12}$$

Then μ^2 of Eq. (6.6) is given by

$$\mu^2 = -m_0^2 + 3\lambda\phi_0^2 \tag{6.13}$$

and since there is only one scalar field in this model

$$\mathcal{M}^2 = -m_0^2 + 3\lambda\phi_0^2 \tag{6.14}$$

https://doi.org/10.1017/9781009290456.007 Published online by Cambridge University Press

Therefore, up to a term that is independent of ϕ_0, the effective potential becomes

$$V_{\text{eff}}(\phi_0, T) = \frac{\bar{m}^2}{2}\phi_0^2 + \frac{\lambda}{4}\phi_0^4 \tag{6.15}$$

with

$$\bar{m}^2 = -m_0^2 + \frac{\lambda}{4}T^2 \tag{6.16}$$

Note that the masses of small excitations around the true vacuum are given by $V''_{\text{eff}}(\phi_0)$ with ϕ_0 being the vacuum expectation value. By minimizing V_{eff} (Eq. (6.15)) we get

$$\phi_{0,\min}(T) = 0, \quad \bar{m}^2 > 0 \tag{6.17}$$

$$= \sqrt{\frac{-\bar{m}^2}{\lambda}}, \quad \bar{m}^2 < 0 \tag{6.18}$$

leading to the mass squared for small excitations (particles) in the true vacuum

$$m_{\text{eff}}^2 \equiv V''_{\text{eff}}(\phi_{0,\min}) = \frac{\lambda}{4}\left(T^2 - T_{\text{c}}^2\right), \quad T > T_{\text{c}} \tag{6.19}$$

$$= \frac{\lambda}{2}\left(T_{\text{c}}^2 - T^2\right), \quad T < T_{\text{c}} \tag{6.20}$$

where T_{c} is the critical temperature

$$T_{\text{c}} = \frac{2m_0}{\sqrt{\lambda}} \tag{6.21}$$

In cosmology, since the universe is expanding, it is also cooling. Therefore we can have one or many cosmological phase transitions and the particle-physics symmetries at high temperatures (early universe) and low temperatures (recent universe) are different. The symmetry after the phase transition can be smaller or larger than the symmetry before the phase transition. In other words, lowering the temperature can spontaneously break or restore a symmetry. We will mostly consider symmetry breaking during the phase transition but examples of symmetry restoration are also easy to construct. A system in which symmetry restoration is observed is Rochelle salt [85, 179].

6.2 Phase dynamics

The effective potential $V_{\text{eff}}(\Phi_0, T)$ is calculated for a system that is in thermal equilibrium, assuming a homogeneous vacuum expectation value of the order parameter Φ_0. Yet thermal equilibrium is not maintained during the phase transition and also the phase change occurs in an inhomogeneous manner. The dynamics are clear

https://doi.org/10.1017/9781009290456.007 Published online by Cambridge University Press

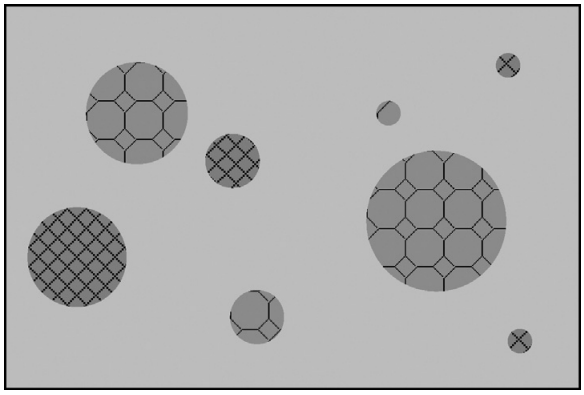

Figure 6.2 A schematic diagram of bubbles nucleating in a first-order phase transition. The two types of bubbles correspond to the two different values of the order parameter. The bubbles grow and collide, and new bubbles nucleate as well. Eventually the whole system is in the new phase.

for a first-order phase transition in which the high temperature phase becomes a metastable state (see Fig. 6.1) at some critical temperature. Now the system can be stuck in this metastable state even when the temperature drops significantly below the critical temperature. An external perturbation can cause the system to transition to the global vacuum. In the absence of an external perturbation, quantum tunneling can trigger the transition. In either case, bubbles of a critical size of the true vacua ($\Phi_0 \neq 0$) nucleate in the false vacuum ($\Phi_0 = 0$) background (see Fig. 6.2). These bubbles grow and eventually merge thus filling space and completing the phase transition. Clearly this process is not homogeneous and cannot be described by an effective potential.

In a second-order transition, in contrast to a first-order transition, there is no metastable state in which the system can be trapped. Thus Φ_0 evolves continuously ("spinodal decomposition") from $\Phi_0 = 0$ to $\Phi_0 \neq 0$. However, different spatial regions evolve at different rates owing to thermal and quantum fluctuations, and Φ_0 is not spatially uniform. Once again, since the effective potential assumes constant Φ_0, it can indicate the existence of a second-order phase transition but cannot be expected to accurately describe the dynamics of the transition. Since defect formation crucially depends on the inhomogeneities of the order parameter during the transition, new ideas have been needed to predict the statistical properties of defects formed in a second-order phase transition.

In one spatial dimension, the distribution of kinks is described by the number density of kinks, and correlators of kink locations. In higher dimensions, the problem becomes richer because domain walls are extended and can curve and have complicated topology. In addition to the mass density in domain walls, we are

https://doi.org/10.1017/9781009290456.007 Published online by Cambridge University Press

interested in the statistical distribution of shapes and sizes of domain walls formed at the phase transition.

6.3 Kibble mechanism: first-order phase transition

At a first-order phase transition, the order parameter has to change from $\Phi_0 = 0$ to its non-zero vacuum expectation value. We are interested in the case when there is more than one possible non-zero value for Φ_0. Then the dynamics in a small spatial region select a vacuum. However the vacuum selected in different spatial regions can be different. For example, in the case of the Z_2 model, the field in a certain region might relax into the $\phi = +\eta$ vacuum, whereas in another region it might relax into $\phi = -\eta$ (see Fig. 6.2).

In a first-order phase transition, each bubble is filled with constant Φ_0 i.e. a fixed vacuum is chosen within a bubble but it can be different for different bubbles. With time, the bubbles grow and collide and fill up the volume. Let us denote by ξ the characteristic size of a region where the same vacuum is selected, after the phase transition is over. Then ξ is the typical size of bubbles when they percolate. If Γ denotes the bubble nucleation rate per unit volume and v is the velocity of the growing bubble walls, then we can define a length scale and a time scale on dimensional grounds (in D spatial dimensions) by

$$\tilde{\xi} = \left(\frac{v}{\Gamma}\right)^{1/(D+1)}, \qquad \tilde{\tau} = \left(\frac{1}{v^D \Gamma}\right)^{1/(D+1)} \tag{6.22}$$

The domain size ξ is a numerical factor times $\tilde{\xi}$ and in practice we take $\xi \sim \tilde{\xi}$. Similarly $\tilde{\tau}$ is related to the time that it takes to complete the phase transition.[2]

The process of bubble percolation has been studied both analytically and numerically [95]. Taking the centers of the bubbles as the vertices of a lattice and connecting only the centers of bubbles that collide, we obtain a random lattice (see Fig. 6.3). We would like to determine the characteristics of such a random lattice since this plays a role in determining the network of defects that form. For example, the typical number of bubbles with which any given bubble collides, also known as the "coordination number" of the random lattice, plays a role in the fraction of closed topological defects (closed domain walls, loops of string, or closely paired monopole-antimonopole pair) that are formed.

In one spatial dimension, every bubble trivially collides with two other bubbles. In two spatial dimensions the average number of collisions is the same as the coordination number of a fully triangulated lattice of infinite extent. From purely

[2] Equation (6.22) relates ξ to the nucleation rate Γ, but it is very hard to measure Γ in any experiment. In fact, it may be easier to measure properties of the defect network, then ξ, and from it infer Γ.

https://doi.org/10.1017/9781009290456.007 Published online by Cambridge University Press

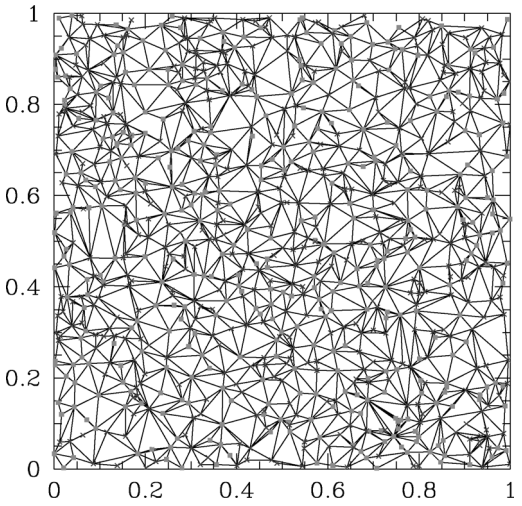

Figure 6.3 If two bubbles collide, their centers are joined by straight lines. The figure then shows the "random bubble lattice" expected in a first-order phase transition in two spatial dimensions.

geometrical constraints that we describe next, the coordination number is six (see, for example, [129]).

The lattice is infinite in extent and by identifying the points at infinity we can view the lattice as lying on a two-dimensional sphere. Then Euler's formula relates the number of vertices (V), edges (E) and faces (F) of the lattice

$$V - E + F = 2 \tag{6.23}$$

Let the coordination number be n. Therefore for every vertex there are n edges but every edge is bounded by two vertices. This relates the number of edges to the number of vertices: $E = nV/2$. Also, every face is a triangle, giving three edges to every face. But an edge is shared by two faces. So $E = 3F/2$. Putting together these relations in Euler's formula gives

$$V - nV/2 + nV/3 = 2 \tag{6.24}$$

In the limit of $V \to \infty$, this yields $n = 6$.

In three spatial dimensions, similar arguments have been given [95] to show that the average coordination number is 13.4. This result is not completely fixed by geometrical constraints as in two dimensions and the result can vary a little depending on the details of the bubble size distribution.

Returning to the $\lambda\phi^4$ model, each bubble either has the phase $\phi_0 = +\eta$ or $\phi_0 = -\eta$ within it. If bubbles of different phases collide, a domain wall forms between the centers of those bubbles. If bubbles of the same phase collide, a wall does not form, though it is possible that a closed domain wall or a wall-antiwall pair forms owing

to the energetics of the bubble collision. We expect small closed walls and closely separated walls and antiwalls to annihilate. Hence the distribution of domain walls after the phase transition is simply described by the locations of bubble collisions when the bubbles carry different phases. Since the phase in the bubbles is $\pm\eta$ with equal probability, the phase transition is simulated by assigning $\pm\eta$ to each of the vertices of the random bubble lattice as in Fig. 6.3. We shall further discuss the properties of the wall network at formation during a first-order phase transition in Section 6.6.

As we have seen, a first-order phase transition is relatively simple to conceptualize. A second-order phase transition is harder to understand. To discuss second-order phase transitions, it is useful to first define an equilibrium correlation length.

6.4 Correlation length

The "equilibrium correlation length," $\bar{\xi}$, is defined as the distance over which field correlations are significant. Generally the field correlations at two spatial points fall off exponentially with increasing separation between the points, $\exp(-r/\bar{\xi})$, and the exponent defines the equilibrium correlation length, $\bar{\xi}$. Hence we need to evaluate the correlation function

$$G(r) = \langle T|\phi(t,\mathbf{x})\phi(t,\mathbf{y})|T\rangle \tag{6.25}$$

where G only depends on $r \equiv |\mathbf{x}-\mathbf{y}|$ because the system is translationally invariant. The thermal state is denoted by $|T\rangle$ and is defined as the state containing the equilibrium number density distribution (Fermi-Dirac or Bose-Einstein) of particles

$$|T\rangle = |\{n_{\mathbf{k}}\}\rangle_T \tag{6.26}$$

$$n_{\mathbf{k}} = \frac{1}{\mathrm{e}^{\beta\omega_k} \pm 1} \tag{6.27}$$

where $\beta \equiv 1/T$ and ω_k is the energy of particles in the $\mathbf{k}$ mode.[3]

With the Z_2 model in mind, we have only one scalar field and the quantum field operator can be expanded in modes about the true vacuum

$$\phi(t,\mathbf{x}) = \phi_0(T) + \int \frac{\mathrm{d}^3k}{(2\pi)^3}\frac{1}{\sqrt{2\omega_k}}\left[\mathrm{e}^{-\mathrm{i}\omega_k t+\mathrm{i}\mathbf{k}\cdot\mathbf{x}}a_{\mathbf{k}} + \mathrm{e}^{+\mathrm{i}\omega_k t-\mathrm{i}\mathbf{k}\cdot\mathbf{x}}a^\dagger_{\mathbf{k}}\right] \tag{6.28}$$

where $\phi_0(T)$ is the vacuum expectation value of the field at temperature T, and $a_{\mathbf{k}}$ and $a^\dagger_{\mathbf{k}}$ are annihilation and creation operators. The dispersion relation is that for a free particle with temperature dependent mass $m(T)$ (see Eq. (6.20) for the $\lambda\phi^4$ model; we have dropped the subscript "eff" for convenience)

$$\omega_k^2 = \mathbf{k}^2 + m^2 \tag{6.29}$$

[3] The chemical potential vanishes in the present case.

https://doi.org/10.1017/9781009290456.007 Published online by Cambridge University Press

The thermal state $|T\rangle$ contains a Bose-Einstein distribution of the particle excitations and the number of scalar particles at momentum $\mathbf{k}$ is given by

$$n_{\mathbf{k}} = \frac{1}{\mathrm{e}^{\beta\omega_k} - 1} \tag{6.30}$$

where $\beta = 1/T$ (Boltzmann constant has been set to 1).

By inserting the expansion in Eq. (6.28) in the correlator, we find

$$G(r) = \int \frac{\mathrm{d}^3k}{(2\pi)^3}\frac{1}{\sqrt{2\omega_k}}\int \frac{\mathrm{d}^3p}{(2\pi)^3}\frac{1}{\sqrt{2\omega_p}}\mathrm{e}^{\mathrm{i}(\mathbf{k}\cdot\mathbf{x}-\mathbf{p}\cdot\mathbf{y})}\langle T|a^\dagger_{\mathbf{k}}a_{\mathbf{p}}|T\rangle + K \tag{6.31}$$

where K is a constant which is independent of temperature and proportional to $\delta^{(3)}(\mathbf{x}-\mathbf{y})$. Then

$$\begin{aligned} G(r) &= \int \frac{\mathrm{d}^3k}{(2\pi)^3}\frac{\mathrm{e}^{-\mathrm{i}\mathbf{k}\cdot(\mathbf{x}-\mathbf{y})}}{\mathrm{e}^{\beta\omega_k}-1} + K \\ &= \frac{T}{4\pi r}\mathrm{e}^{-m(T)r} + K \end{aligned} \tag{6.32}$$

where, in doing the integral, we have assumed $m(T) \ll T$. From the final expression we get the equilibrium correlation length

$$\bar{\xi} = \frac{1}{m(T)} \tag{6.33}$$

For the Z_2 model (Eq. (6.20))

$$m^2 = \frac{\lambda}{4}\left(T^2 - T_{\mathrm{c}}^2\right), \quad T > T_{\mathrm{c}} \tag{6.34}$$

$$= \frac{\lambda}{2}\left(T_{\mathrm{c}}^2 - T^2\right), \quad T < T_{\mathrm{c}} \tag{6.35}$$

Therefore the equilibrium correlation length is

$$\bar{\xi}(T) = \sqrt{\frac{4}{\lambda}}\frac{1}{\sqrt{T^2 - T_{\mathrm{c}}^2}}, \quad T > T_{\mathrm{c}} \tag{6.36}$$

$$= \sqrt{\frac{2}{\lambda}}\frac{1}{\sqrt{T_{\mathrm{c}}^2 - T^2}}, \quad T < T_{\mathrm{c}} \tag{6.37}$$

or

$$\bar{\xi}(T) \propto |T - T_{\mathrm{c}}|^{-1/2} \tag{6.38}$$

The essential feature in $\bar{\xi}$ is the singularity at $T = T_{\mathrm{c}}$, that occurs at a time that we denote t_{c}. Assuming that the cooling (quench) occurs at a constant rate $T_{\mathrm{c}}/\tau_{\mathrm{ext}}$ (in a range of temperature around T_{c}), we have

$$T - T_{\mathrm{c}} = -\frac{T_{\mathrm{c}}}{\tau_{\mathrm{ext}}}(t - t_{\mathrm{c}}) \tag{6.39}$$

https://doi.org/10.1017/9781009290456.007 Published online by Cambridge University Press

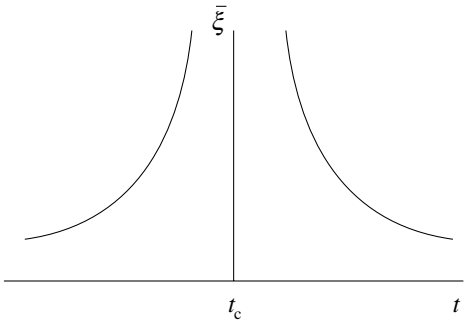

Figure 6.4 Sketch of equilibrium correlation length as a function of time as given in Eq. (6.40).

hence we write

$$\bar{\xi} \sim |T - T_c|^{-\nu} \propto |t - t_c|^{-\nu} \tag{6.40}$$

for T close to T_c. The exponent ν is called a "critical exponent" and the mean field theory calculation described above gives $\nu = 1/2$. However, the mean field theory ignores particle interactions and renormalization group methods give $\nu = 2/3$, which is closer to experiment. A sketch of the shape of $\bar{\xi}$ (Eq. (6.40)) is shown in Fig. 6.4.

One shortcoming of the mean field calculation of $\bar{\xi}$ is that we have quantized the field ϕ in a fixed true vacuum so that $\phi_0(T)$ in Eq. (6.28) is independent of x. This assumes that the same vacuum is chosen everywhere below T_c. On the other hand, we are precisely interested in the spatial extent of a region in a single vacuum. Hence a more suitable expansion of ϕ would be

$$\phi(t, \mathbf{x}) = \phi_0(t, \mathbf{x}, T) + \int \frac{\mathrm{d}^3k}{(2\pi)^3} \frac{1}{\sqrt{2\omega_k}} \left[f_k(t, x) a_{\mathbf{k}} + f_k^*(t, x) a_{\mathbf{k}}^\dagger \right] \tag{6.41}$$

instead of Eq. (6.28). The vacuum expectation value, ϕ_0, is now allowed to depend on both t and x since the background domain walls may be non-static. The second term in the expansion describes small fluctuations (particles) with mode functions f_k in the classical background $\phi_0(t, x, T)$ at x.

The expansion in Eq. (6.41) is not as obvious as might appear at first sight. We have seen in Chapter 4 that a kink can itself be written in terms of particles via the Mandelstam operator. This was done in the sine-Gordon model but it is conceivable that such an operator also exists in other models. So the above expansion only makes sense for a state in which there is a clear separation between the particle degrees of freedom appearing in the sum and the soliton degrees of freedom included in ϕ_0. For example, if the walls are very close to each other the separation of the two

terms may not be justified. Hence the phenomenon of defect formation is closely tied to the separation of classical (soliton) and quantum (particle) variables.

We are interested in

$$\xi_0 = \langle T|\phi_0(t, x, T)\phi_0(t, y, T)|T\rangle \tag{6.42}$$

However, we have no way of calculating this equal time "domain correlation function" since (i) the thermal state refers to a thermal distribution of particles, not of domains, and (ii) the defects do not remain in thermal equilibrium with the particles. This impasse is made less severe by realizing that the calculation of $\bar{\xi}$ for $T > T_c$ does not suffer from this problem since then $\phi_0 = 0$ is the unique vacuum. We expect the correlations for $T < T_c$ to be determined by those for $T > T_c$ and so it might be sufficient to know the correlation length for $T > T_c$. (We discuss this further in Section 6.5.) To emphasize this point, the two branches of the sketch in Fig. 6.4 correspond to two different quantities – the equilibrium correlation length for $t < t_c$ is for excitations in a different vacuum from that for $t > t_c$. So, while Eq. (6.40) describes the correlations of particle excitations in a given true vacuum for $T < T_c$ ($t > t_c$), we cannot expect that this has anything to do with the size of domains of constant vacuum.

The next subtlety is that the divergence of the equilibrium correlation length at $T = T_c$ should not be taken too literally. The reason is that there is an external agency (refrigerator) driving the phase transition on a time scale given by τ_{ext}. As the system gets closer to the critical temperature, it takes longer for equilibrium to be established, while the external agency continues to cool the system at a rate determined by external factors. At some temperature above the critical temperature the time taken to maintain equilibrium becomes larger than the time scale at which the external conditions are changing.

Assume that the external temperature is being lowered at a constant rate

$$T = T_c\left(1 - \frac{t}{\tau_{ext}}\right) \tag{6.43}$$

where T_c is the critical temperature and we have chosen $T_c = 0$ for convenience. The equilibrium correlation length has the form

$$\bar{\xi}(T) = \eta|\epsilon|^{-\nu} \tag{6.44}$$

where ν is a critical exponent, η is some unspecified length scale, and

$$\epsilon \equiv 1 - \frac{T}{T_c} \tag{6.45}$$

The rate of change of $\bar{\xi}$ is

$$\frac{d\bar{\xi}}{dt} = -\frac{\epsilon}{|\epsilon|}\frac{\nu\eta}{\tau_{ext}}|\epsilon|^{-(\nu+1)} = -\frac{\nu\bar{\xi}}{\tau_{ext}\epsilon} \tag{6.46}$$

https://doi.org/10.1017/9781009290456.007 Published online by Cambridge University Press

This equation shows that as $\epsilon \to 0-$, $\bar{\xi}$ must change at an ever faster rate if equilibrium is to be maintained.

The relaxation rate can be obtained by perturbing the system and finding how long it takes for the perturbation ("sound") to equilibrate. The result is the "relaxation time"

$$\tau_{\rm rel} = \tau_0 |\epsilon|^{-\mu} \tag{6.47}$$

where μ is another critical exponent. Then the "speed of relaxation" is the sound speed

$$c_{\rm s}(T) = \frac{\bar{\xi}}{\tau_{\rm rel}} = \frac{\eta}{\tau_0} |\epsilon|^{\mu-\nu} \tag{6.48}$$

Note that $\tau_{\rm rel}$ diverges as T approaches $T_{\rm c}$. This is called "critical slowing down." When the system cannot keep up with the external changes, equilibrium is lost. Denoting the temperature at which $\tau_{\rm rel}$ becomes equal to $\tau_{\rm ext}$ by T_* we find

$$T_* = T_{\rm c} \left[1 + \left(\frac{\nu \tau_0}{\tau_{\rm ext}} \right)^{1/(\mu+1)} \right] \tag{6.49}$$

which occurs at

$$t_* = -\tau_{\rm ext} \left(\frac{\nu \tau_0}{\tau_{\rm ext}} \right)^{1/(\mu+1)} \tag{6.50}$$

So we expect the correlation length ξ for $T > T_{\rm c}$ to be equal to the equilibrium correlation length $\bar{\xi}$ until time t_*, after which ξ departs from $\bar{\xi}$ and grows more slowly (see Fig. 6.5). The behavior of ξ between t_* and $t_{\rm c}$ is not known and it is generally assumed that ξ does not change very much in this interval. After $t_{\rm c}$, there are two distinct vacua, and we need to consider both the correlation scale of chosen vacua (denoted by ξ_0) and the correlations of excitations within a chosen vacuum, ξ. As time goes by, walls annihilate and the domain size with a given vacuum grows. We discuss ξ_0 in the next section.

6.5 Kibble-Zurek mechanism: second-order phase transition

The domain correlation length, ξ_0, over which the same vacuum is chosen, is different from the equilibrium correlation length denoted by $\bar{\xi}$ (Eq. (6.40)). It is also different from the correlation length ξ obtained for particle excitations, including the phenomenon of critical slow down, since ξ_0 has nothing to do with particle excitations. We now discuss different approaches to estimating ξ_0 (for a review see [10]).

https://doi.org/10.1017/9781009290456.007 Published online by Cambridge University Press

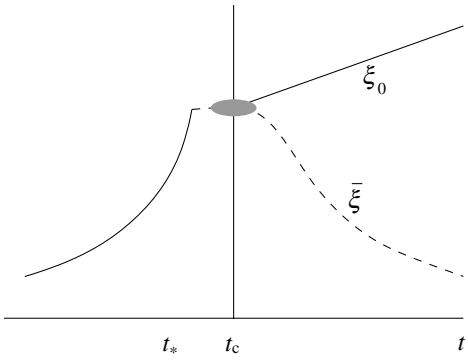

Figure 6.5 The correlation length at high temperature ($t < t_c$) increases as the critical temperature is approached, departing from the equilibrium correlation length when critical slowing down becomes important at t_*. Below the critical temperature, there are two correlation length scales of interest. The domain correlation length, ξ_0, relates to the extent of the spatial domains that are in the same vacuum. This is precisely the spacing of domain walls. Wall-antiwall annihilations cause ξ_0 to grow with time. The particle correlation length, ξ, however, decreases with time since the mass of the particles grows, and eventually approaches the zero temperature value. The dynamics of how ξ_0 separates from $\bar{\xi}$ are not understood and are denoted by the shaded region.

To estimate ξ_0 in the case of a second-order phase transition, Kibble [87] used two different criteria. First, he obtained an upper bound to ξ_0 in the cosmological context based on causality considerations. If the phase transition takes place at a certain cosmic time τ, then the vacua at points separated by more than $c\tau$, where c is the speed of light, must have been selected independently since $c\tau$ is the size of the cosmic horizon. Hence $\xi < c\tau$. This is the "causality bound."

The second estimate is based on finding the Ginzburg length. This is the length over which the choice of vacuum cannot change owing to thermal fluctuations. For concreteness, let us imagine that there is a domain of size l in which $\phi = +\phi_0(T)$ ($T < T_c$) in the Z_2 model. In one spatial dimension this corresponds to a wall-antiwall separated by a distance l, and in three dimensions it corresponds to a closed domain wall of characteristic size l. The idea is that, if l is small, thermal fluctuations can spontaneously change the phase within the domain from $\phi = +\phi_0$ to $\phi = -\phi_0$. However, if l is large, the phase in the domain is frozen, and the distribution of defects does not change spontaneously owing to thermal fluctuations. The smallest length l for which a domain is frozen defines the distance between closest defects and hence predicts the number density of defects.

The energy required to change the phase in a volume R^3 is given by $R^3 \Delta V(T)$ where ΔV is the free energy density difference between the minimum and maximum of the potential at a temperature T. The thermal fluctuation energy available per

https://doi.org/10.1017/9781009290456.007 Published online by Cambridge University Press

excitation mode is T according to equipartition. Equating the required and the available energies gives

$$R^3 \Delta V(T) \approx T \tag{6.51}$$

Therefore, at temperature $T < T_c$, a region that is smaller than

$$R \sim \left(\frac{T}{\Delta V(T)} \right)^{1/3} \tag{6.52}$$

will have enough thermal energy to fluctuate from one vacuum to the other. For example, in the Z_2 model (see Eq. (6.15))

$$\Delta V(T) = \frac{\bar{m}^4}{4\lambda} = \frac{\lambda}{64} \left(T^2 - T_c^2 \right)^2 \tag{6.53}$$

Therefore, at temperature $T < T_c$, the length scale below which regions are still fluctuating are

$$R(T) = \frac{4}{\lambda^{1/3}} \left[\frac{T}{\left(T_c^2 - T^2 \right)^2} \right]^{1/3} \sim \frac{4^{2/3}}{\lambda^{1/3} T_c} \left[1 - \frac{T}{T_c} \right]^{-2/3} \tag{6.54}$$

where the last approximation holds for $T \sim T_c$.

For a region to fluctuate from one vacuum to another, not only does it need the energy to jump over the barrier, but all different parts of the region need to jump together. This means that all the particles in the domain should be activated coherently. The particle coherence scale is described by the correlation length, which is approximated by the equilibrium correlation length, $\bar{\xi}$. Therefore, at a temperature T, regions of size less than $l_f = \min(R(T), \bar{\xi}(T))$ (subscript "f" stands for "fluctuating") can actively change vacua. The Ginzburg temperature, T_G, is defined by the condition $R(T_G) = \bar{\xi}(T_G)$, and the Ginzburg length is defined by $l_G = \bar{\xi}(T_G)$. For the Z_2 model, this gives

$$T_c - T_G \approx \lambda T_c \tag{6.55}$$

$$l_G = \bar{\xi}(T_G) \approx \frac{1}{\lambda T_c} \tag{6.56}$$

Early estimates took the Ginzburg temperature to be the epoch when domain walls are formed. The number density of walls then follows by dimensional analysis as $\sim 1/l_G^D$.

The relevance of the Ginzburg temperature for defect formation is not clear. As discussed in the previous section, the correlation length $\bar{\xi}$ is calculated for particle excitations in a given vacuum, whereas we are interested in the correlation length of the vacuum domains denoted by ξ_0. In fact, experiments in He-3 find that defects are produced at a temperature below T_c but above T_G, implying that the Ginzburg

https://doi.org/10.1017/9781009290456.007 Published online by Cambridge University Press

criterion is not a necessary condition for defect formation. A discussion of the relevance of the Ginzburg criterion in the context of vortex formation in He-3 and He-4 may be found in [86].

Zurek estimated the domain size, ξ_Z, by considering the time scales involved during the phase transition [187, 188, 93]. As discussed at the end of Section 6.4, the system cannot keep up with external changes at $t = t_*$ (Fig. 6.5). Zurek postulated that the correlation length at the instant when the system can no longer keep up with the external changes determines the size of the domains that get frozen. This in turn determines the number of defects.

To estimate ξ_0 at t_c we know $\bar{\xi}$ at the time critical slowing down becomes important. To this we add the distance that a perturbation can propagate from the slow-down time, t_*, to the phase transition time, t_c (see Fig. 6.5). That gives us

$$\xi_0(t_c) = \bar{\xi}(t_*) + \int_{t_*}^{t_c} \mathrm{d}t\ c_s(t) \tag{6.57}$$

$$= \eta \frac{1+\mu}{1+\mu-\nu} \left(\frac{\tau_{\text{ext}}}{\nu \tau_0} \right)^{\nu/(1+\mu)} \tag{6.58}$$

The crucial part of this relation is

$$\xi_0(t_c) \propto \left(\frac{\tau_{\text{ext}}}{\tau_0} \right)^{\nu/(1+\mu)} \tag{6.59}$$

This relation gives the dependence of the number density of domain walls in D spatial dimensions on the external time

$$n \propto \left(\frac{\tau_{\text{ext}}}{\tau_0} \right)^{-\nu D/(1+\mu)} \tag{6.60}$$

We can control τ_{ext} in experiments and hence this is a testable prediction.

The above analysis can be improved yet further. For example, we have calculated ξ_0 at $t = t_c$. Yet thermal fluctuations after $t = t_c$ (i.e. $T < T_c$) may be important and the domain structure may freeze out at yet lower temperatures, as in the discussion of the Ginzburg length scale above. So the relevant time at which ξ_0 is stable to thermal fluctuations is somewhat after t_c, in agreement with the analysis of [8].

There is yet another view of defect formation at a phase transition first proposed in [5]. In numerical simulations of a $U(1)$ field theory, the authors found that there is a distribution of vortices even at temperatures above the phase transition. However, these vortices are small, closed structures. At the critical temperature, the vortices link up and form infinite, open structures. Thus the phase transition is coincident with a percolation transition of the vortices. If this feature is generally true, we expect a population of small, closed domain walls to exist above the critical temperature. As the temperature is lowered, the walls connect and grow larger and

Table 6.1 *Size distribution of black clusters found by simulations on a cubic lattice.*

Cluster size	1	2	3	4	6	10	31 082
Number	462	84	14	13	1	1	1

at the critical temperature, the walls percolate, giving walls of infinite extent. The percolation picture has not been checked by simulating the domain wall forming phase transition. However, we can still study the statistical properties of the network of walls formed after a phase transition using some simple arguments that we now describe.

The topic of defect formation and, more generally, phase transition dynamics is still under active investigation.

6.6 Domain wall network formation

The previous sections focused on the density of domain walls that can be expected to form during a suitable phase transition. In this section we focus on a somewhat different aspect of the problem: what are the statistical properties of the domain walls formed at a phase transition? Are the domain walls formed as little closed spherical structures? Or are they infinite and planar? First we discuss the simple case of a network of Z_2 walls and then the more complicated case of $SU(5) \times Z_2$ walls.

6.6.1 Z_2 network

The properties of the network of Z_2 domain walls at formation have been determined by numerical simulations implementing the "Kibble mechanism." The vacuum in any correlated region of space is determined at random. Then, if there are only two degenerate vacua (call them black and white), there are spatial regions that are in the black phase with 50% probability and others in the white phase. The boundaries between these regions of different phases are the locations of the domain walls (see Fig. 6.6).

Numerical simulations of the Kibble mechanism on a cubic lattice gave the statistics shown in Table 6.1 [74, 159]. The data show that there is essentially one giant connected black cluster. By symmetry there is one connected white cluster. In the infinite volume limit, these clusters are also infinite and their surface areas are infinite. Therefore the topological domain wall formed at the phase transition is infinite.

https://doi.org/10.1017/9781009290456.007 Published online by Cambridge University Press

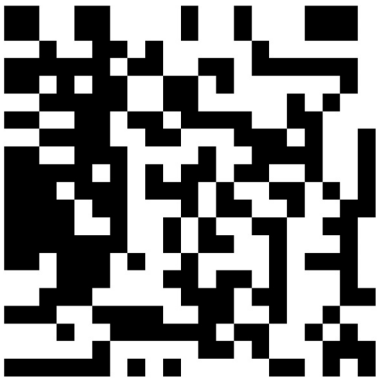

Figure 6.6 The distribution of two phases (black and white) on a square lattice in two spatial dimensions. Domain walls lie at the interface of the black and white regions.

6.6.2 $SU(5)$ *network*

What does the Kibble mechanism predict for $SU(5) \times Z_2$ domain walls? Just as in the Z_2 case, we have to throw down values of the Higgs field on a lattice, assuming that every point on the vacuum manifold is equally likely, and then examine the walls that would form at the interface. In Section 2.2 we have found that there are three kinds of wall solutions in this model and we have labeled the walls by the index q, which can take values 0, 1, or 2. Each kind of wall has the same topology but they have different masses. Each wall type is formed with some probability. Based on the Kibble mechanism, the probability that a certain wall forms is directly related to the number of boundary values that result in the formation of that kind of wall. So we need to evaluate all the boundary conditions that lead to domain walls with a certain value of q.

The space of boundary conditions leading to a given type of domain wall is discussed in Section 2.4. However, similar considerations occur in simpler models and it is helpful to think of the problem in a discrete case, for example the $S_5 \times Z_2$ kinks described in Section 2.5. Take a fixed (discrete) vacuum in one domain. The neighboring domain can be in any other vacuum state with equal probability. There are ten possible states for the neighboring domain. Only one of these gives the $q = 0$ wall, six give the $q = 1$ wall, and three give the $q = 2$ wall. Then the Kibble mechanism implies that the network contains $q = 0, 1, 2$ walls and their number densities are in the ratio $1 : 6 : 3$. This means that the network is dominantly composed of the $q = 1$ wall. However, since the $q = 2$ wall is the lightest wall, the $q = 1$ walls formed by the Kibble mechanism during the phase transition subsequently decay into $q = 2$ walls. We will show some evidence for this two-stage process in Section 6.7.

https://doi.org/10.1017/9781009290456.007 Published online by Cambridge University Press

Similarly we can identify the space of boundary conditions that lead to a particular kind of kink in the $SU(5) \times Z_2$ model. We considered this problem in Section 2.4 and listed the spaces in Table 2.1. From the table we read off that the space of boundary conditions leading to the $q = 0$ kink is zero dimensional, for the $q = 1$ kink it is six dimensional, and is four dimensional for the $q = 2$ kink. Since a six-dimensional space is infinitely bigger than a 0- or a four-dimensional space, the probability of a kink being of the $q = 0$ or $q = 2$ variety is zero, and the probability of the kink being of the $q = 1$ variety is 1.

A subtlety that has not been discussed above is that there is also the possibility that if we lay down Higgs fields randomly, we may get $[\Phi_-, \Phi_+] \neq 0$ (see theorem in Section 2.2). In this case, as described in Section 2.2, there is no static solution to the equations. Then the field configuration evolves toward a static configuration. Our discussion above assumes that such a configuration has been reached, and neighboring domains always have values of Φ that commute. This is not completely satisfactory since there are time scales that are associated with the relaxation and these must be compared to other time scales characterizing the phase transition. This is why a numerical study, such as that in Section 6.7, is needed.

To summarize, the Kibble mechanism predicts that only $q = 1$ domain walls are formed at the $SU(5) \times Z_2$ phase transition. However, we know that the stable variety of walls have $q = 2$, and hence the $q = 1$ walls decay into them. The formation of walls and the conversion of $q = 1$ walls into $q = 2$ walls during a phase transformation in the $SU(5) \times Z_2$ model has not been studied. However, these questions have been addressed in the related $S_5 \times Z_2$ model as we now discuss.

6.7 Formation of $S_5 \times Z_2$ domain wall network

As discussed in the last section, the $q = 1$ domain wall of the $S_5 \times Z_2$ model occupies the largest volume in the space of boundary conditions but the $q = 2$ wall has least energy. Hence there is a tension between "entropy" (number of states) and "energy" (mass of wall). In a phase transition, based on the Kibble argument, we might expect the entropy to be more important. However, the higher energy walls $q = 1$ cannot survive indefinitely and eventually decay into the $q = 2$ walls. One way to study these processes is by direct simulation of the fields as a function of temperature [123, 6, 7].

The simulations are based on a Langevin equation where thermal effects are treated as a noise term in the classical equations of motion together with a damping term. For the $S_5 \times Z_2$ model (Eq. (2.30)) with its four scalar fields, the equations are

$$\left(\partial_t^2 - \nabla^2\right) f_i + V_i + \Delta\, \partial_t f_i = \Gamma_i \tag{6.61}$$

https://doi.org/10.1017/9781009290456.007 Published online by Cambridge University Press

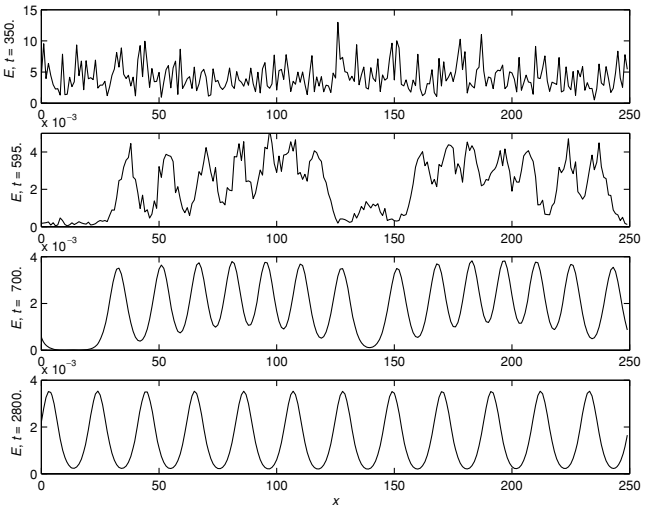

Figure 6.7 Energy density distribution in space at an early time at high temperature (top panel) and then at various times after the phase transition in the lower panels. The last panel shows that the system has relaxed into a stable lattice of kinks.

where $i = 1, \ldots, 4$ and V_i denotes the derivative of V with respect to f_i. If $\Delta = 0 = \Gamma_i$, these equations are simply the classical equations of motion for the f_i. In a thermal system, we imagine that the fields are in contact with a heat bath at temperature T with which energy can be exchanged. Then there can be dissipation which is represented by the Δ term and thermal noise which is represented by the Γ_i term. The dissipation constant Δ is taken to be independent of the temperature but the Γ_i are stochastic and taken to be Gaussian distributed with the following correlation functions

$$\begin{aligned} &\langle \Gamma_i(\mathbf{x}, t) \rangle = 0, \\ &\langle \Gamma_i(\mathbf{x}, t) \Gamma_j(\mathbf{y}, t') \rangle = 2\Delta \; T \; \delta_{ij} \delta(\mathbf{x} - \mathbf{y}) \delta(t - t') \end{aligned} \tag{6.62}$$

The procedure is to solve Eq. (6.61) with any initial condition. The noise and dissipation eventually drive the system to a thermal distribution at temperature T. To mimic the phase transition, the noise is then set to zero. All of a sudden the system has to find a new equilibrium state. This equilibrium state has domain walls and these are located and tracked in the subsequent evolution.

In one spatial dimension, the results are shown in Fig. 6.7. At high temperature the energy distribution is very noisy. After the phase transition, the presence of kinks is clear. During the evolution, some of these kinks annihilate. In the end we are left with a kink lattice.

https://doi.org/10.1017/9781009290456.007 Published online by Cambridge University Press

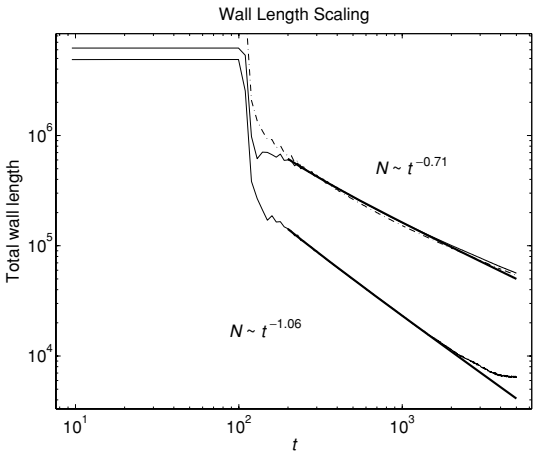

Figure 6.8 Length in walls (denoted by N) in two spatial dimensions against time for the $q = 2$ walls in the $S_5 \times Z_2$ model (upper solid curve) and the single field Z_2 case (lower solid curve). The dashed curve corresponds to the total $S_5 \times Z_2$ wall length measured by counting zeros of the diagonal elements of $\Phi(x)$ and hence includes walls with any value of q. The difference between the solid and dashed curves shows that the initial network consists of a large fraction of $q \neq 2$ walls but then later all the walls decay into the $q = 2$ walls. Comparison with the Z_2 case shows that the $S_5 \times Z_2$ network decays more slowly. (The upturn at the very end in the Z_2 case is due to the finite simulation box.)

Similar numerical simulations have also been done in two spatial dimensions. The total energy in all kinds of walls is plotted as a function of time in Fig. 6.8. The figure also shows the energy in only the $q = 2$ walls as a function of time. The difference of these curves shows that not all walls are of the $q = 2$ variety at formation. Other kinds of walls are present immediately after the phase transition but they must then decay into the least massive $q = 2$ wall.

As discussed in Section 2.8, the $S_5 \times Z_2$ kinks can have nodes in two spatial dimensions (see Fig. 2.6). So we expect a network of domain walls to form after a phase transition in which six or more domain walls are joined at junctions. This is exactly what is seen in simulations (Fig. 6.9). Another feature that is apparent on a closer look at the network is that there are many pairs of walls that are very close to each other. These pairs occur because the unstable $q = 1$ walls eventually decay into two $q = 2$ walls. The forces separating the $q = 2$ walls are exponentially small and so they stay close-by during further evolution.

We have seen that the final state of the $S_5 \times Z_2$ phase transition in one spatial dimension is a lattice of domain walls (Fig. 6.7). In one dimension, it can be argued that a lattice forms with unit probability provided the size of the simulation box is much larger than the wall thickness. In two dimensions, if the spatial extent in one

https://doi.org/10.1017/9781009290456.007 Published online by Cambridge University Press

Figure 6.9 Network of $S_5 \times Z_2$ walls in two spatial dimensions soon after the phase transition. The picture looks very similar to the network of (one-dimensional) walls connected to a network of (point-like) strings studied in [130].

direction is smaller than that in the other direction, so that the simulation box is rectangular with periodic boundary conditions, the evolution is very much like in one dimension and a lattice forms once again (see Fig. 6.10). Even on a square two-dimensional simulation box, a domain wall lattice is seen to form with a probability ~ 0.05 [7].

6.8 Biased phase transitions

The existence of domain walls relies only on the existence of discrete vacua. Then it is possible to imagine situations where the degeneracy of the discrete vacua is slightly broken (see Fig. 6.11).[4] Now the probability that the higher energy vacuum is selected during the phase transition in some region is less than $1/2$ and the probability that the lower energy vacuum is selected is larger than $1/2$. This process can again be simulated on a square lattice by throwing down black squares with probability $p < 1/2$. If p is very small, there are only a few black squares and these are disconnected from each other. So the domain walls are small

[4] Or perhaps the vacua are exactly degenerate but the likelihood of being in one particular vacuum is slightly larger because of the way in which the system was prepared.

https://doi.org/10.1017/9781009290456.007 Published online by Cambridge University Press

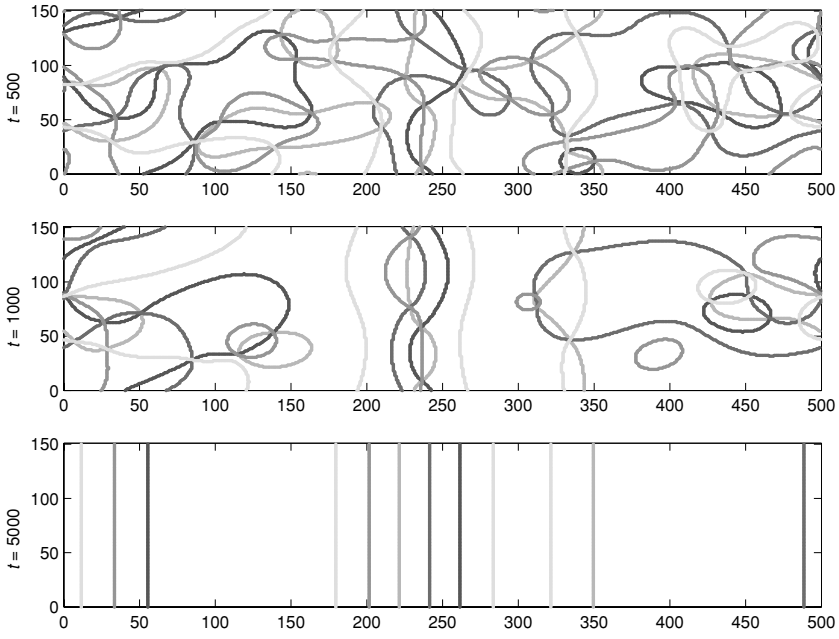

Figure 6.10 Three stages for the domain wall network evolution in a toroidal domain, with dimensions $L_x = 500$ and $L_y = 150$. The different shades correspond to the five possible charges of the domain walls (see Section 2.7). Note that in the bottom figure there is a pair of neighboring wall and antiwall of the same type (the walls just before and after the 300 mark). These later annihilate, leading to a final stable lattice consisting of ten walls.

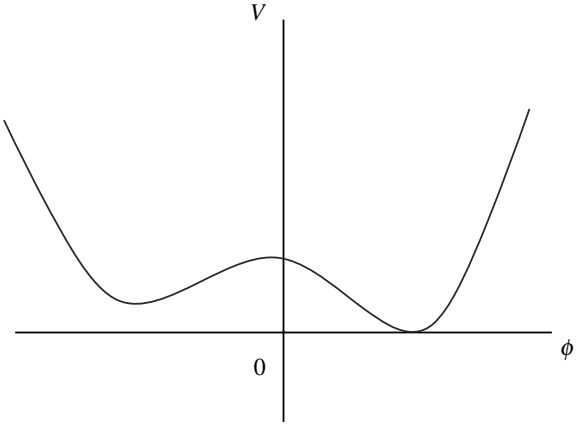

Figure 6.11 An asymmetric well in which the degeneracy of the vacua is slightly broken.

https://doi.org/10.1017/9781009290456.007 Published online by Cambridge University Press

and closed. At a critical value of p, call it p_c, the black squares connect and the distribution is dominated by one infinite cluster of black squares. Then the black squares are said to percolate. Therefore the domain wall formation problem reduces to the classic problem of "percolation theory" [143, 96, 36] where we are interested in the critical probability and also the critical exponents that appear in various correlation functions as the critical point is approached. On a triangular lattice in two dimensions, the critical probability is known to be 0.5 and on a cubic lattice in three dimensions it is 0.31. The problem may even be studied on a random lattice as discussed in [95].

The analysis for biased domain walls implies that even if the potential is slightly asymmetric, infinite domain walls can form. For the $SU(5) \times Z_2$ potential described in Eq. (2.5), the asymmetry is due to the cubic term with coupling constant, γ. For small but non-zero values of γ, infinite domain walls form.

6.9 Open questions

1. What is the number density of domain walls formed in a second-order phase transition? The question may need to be sharpened since the density keeps changing with time. Also, while the number density is important in cosmology, condensed matter physicists are mainly concerned with scaling laws (critical exponents) since these are expected to be universal. So a sharper question would be in terms of a critical exponent related to the number density (e.g. Eq. (6.60)).
2. Is there a condensed matter system which gives a domain wall lattice?
3. Is there any role for domain wall lattices in (higher dimensional) cosmology?
4. If a domain wall lattice can be generalized to strings and monopoles, do string and monopole lattices form during a phase transition?

https://doi.org/10.1017/9781009290456.007 Published online by Cambridge University Press